TU Delft

Delft University of Technology

Charge Transfer and Asymmetric Coupling of $MoSe_2$ Valleys to the Magnetic Order of CrSBr

Serati de Brito, Caique; Faria Junior, Paulo E.; Ghiasi, Talieh S.; Ingla-Aynés, Josep; Rabahi, César Ricardo; Cavalini, Camila; Mañas-Valero, Samuel; Taniguchi, Takashi; van der Zant, Herre S.J.; More Authors

DOI
10.1021/acs.nanolett.3c03431

Publication date
2023

Document Version
Final published version

Published in
Nano Letters

Citation (APA)
Serati de Brito, C., Faria Junior, P. E., Ghiasi, T. S., Ingla-Aynés, J., Rabahi, C. R., Cavalini, C., Mañas-Valero, S., Taniguchi, T., van der Zant, H. S. J., & More Authors (2023). Charge Transfer and Asymmetric Coupling of $MoSe_2$ Valleys to the Magnetic Order of CrSBr. *Nano Letters*, *23*(23), 11073-11081. https://doi.org/10.1021/acs.nanolett.3c03431

Important note
To cite this publication, please use the final published version (if applicable).
Please check the document version above.

Copyright
Other than for strictly personal use, it is not permitted to download, forward or distribute the text or part of it, without the consent of the author(s) and/or copyright holder(s), unless the work is under an open content license such as Creative Commons.

Takedown policy
Please contact us and provide details if you believe this document breaches copyrights.
We will remove access to the work immediately and investigate your claim.

This work is downloaded from Delft University of Technology.
For technical reasons the number of authors shown on this cover page is limited to a maximum of 10.

NANO LETTERS

pubs.acs.org/NanoLett Letter

Charge Transfer and Asymmetric Coupling of $MoSe_2$ Valleys to the Magnetic Order of CrSBr

Caique Serati de Brito, Paulo E. Faria Junior, Talieh S. Ghiasi, Josep Ingla-Aynés, César Ricardo Rabahi, Camila Cavalini, Florian Dirnberger, Samuel Mañas-Valero, Kenji Watanabe, Takashi Taniguchi, Klaus Zollner, Jaroslav Fabian, Christian Schüller, Herre S. J. van der Zant, and Yara Galvão Gobato*

Cite This: *Nano Lett.* 2023, 23, 11073–11081 Read Online

ACCESS | Metrics & More | Article Recommendations | Supporting Information

ABSTRACT: van der Waals heterostructures composed of two-dimensional (2D) transition metal dichalcogenides and vdW magnetic materials offer an intriguing platform to functionalize valley and excitonic properties in nonmagnetic TMDs. Here, we report magneto photoluminescence (PL) investigations of monolayer (ML) $MoSe_2$ on the layered A-type antiferromagnetic (AFM) semiconductor CrSBr under different magnetic field orientations. Our results reveal a clear influence of the CrSBr magnetic order on the optical properties of $MoSe_2$, such as an anomalous linear-polarization dependence, changes of the exciton/trion energies, a magnetic-field dependence of the PL intensities, and a valley *g*-factor with signatures of an asymmetric magnetic proximity interaction. Furthermore, first-principles calculations suggest that $MoSe_2$/CrSBr forms a broken-gap (type-III) band alignment, facilitating charge transfer processes. The work establishes that antiferromagnetic–nonmagnetic interfaces can be used to control the valley and excitonic properties of TMDs, relevant for the development of opto-spintronics devices.

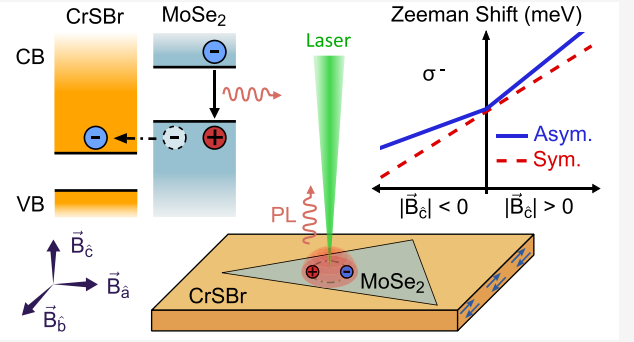

KEYWORDS: *transition metal dichalcogenides, two-dimensional magnets, van der Waals heterostructures, proximity effects, magneto-optics*

Downloaded via TU DELFT on December 21, 2023 at 17:46:21 (UTC).
See https://pubs.acs.org/sharingguidelines for options on how to legitimately share published articles.

Recently, van der Waals (vdW) magnetic materials have attracted increasing attention because of their unique magnetic properties and possible applications in spintronics.[1−13] Several studies were performed in heterostructures using magnetic materials and monolayer transition metal dichalcogenides (TMDs).[1−3,14−22] These heterostructures employ magnetic proximity effects to modify the physical properties of the ML TMD adjacent to the magnetic material and therefore offer new opportunities for engineering magnetic heterostructures.[18] Actually, recent studies evidenced an enhanced valley splitting of WSe_2 and WS_2 monolayers on the ferromagnetic (FM) material EuS,[23,24] a giant zero-field valley splitting of $MoSe_2/CrBr_3$,[25] asymmetric magnetic proximity interactions in $MoSe_2/CrBr_3$,[16] and an anomalous temperature dependence of the $MoSe_2/MnPSe_3$ excitonic peak below the Néel temperature (T_N).[3] Furthermore, magnetic proximity effects have led to spin-dependent charge transfer and concomitant circularly polarized PL in hybrid devices based on both CrI_3[2,17] and $CrBr_3$.[1] However, most previous studies in magnetic vdW heterointerfaces involved vdW ferromagnetic materials.[1−6] AFM materials have a variety of spin orderings with distinct magnetic symmetry groups which could result in unique magnetic properties, and therefore there are interesting ways to control their functionalities by choosing appropriate AFM materials.[3]

In this work, we investigate the impact of the CrSBr antiferromagnetic substrate on the exciton and valley properties of ML $MoSe_2$. We performed micro-PL measurements under a magnetic field along each of the three crystallographic axes of CrSBr. In general, our findings show that the exciton and valley properties of ML TMDs can be engineered by the interplay of magnetic proximity, efficient charge transfer effects, exciton/trion–magnon coupling, and dielectric anomalies of 2D antiferromagnetic materials.

The layered magnetic material CrSBr is a vdW direct gap semiconductor with A-type AFM and Neél temperature of 132 K in its bulk form.[26−34] In addition, CrSBr presents another phase transition around the temperature of T = 40 K[7,29,30]

Received: September 7, 2023
Revised: November 20, 2023
Accepted: November 20, 2023
Published: November 29, 2023

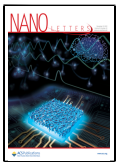

ACS Publications © 2023 American Chemical Society

https://doi.org/10.1021/acs.nanolett.3c03431
Nano Lett. 2023, 23, 11073–11081

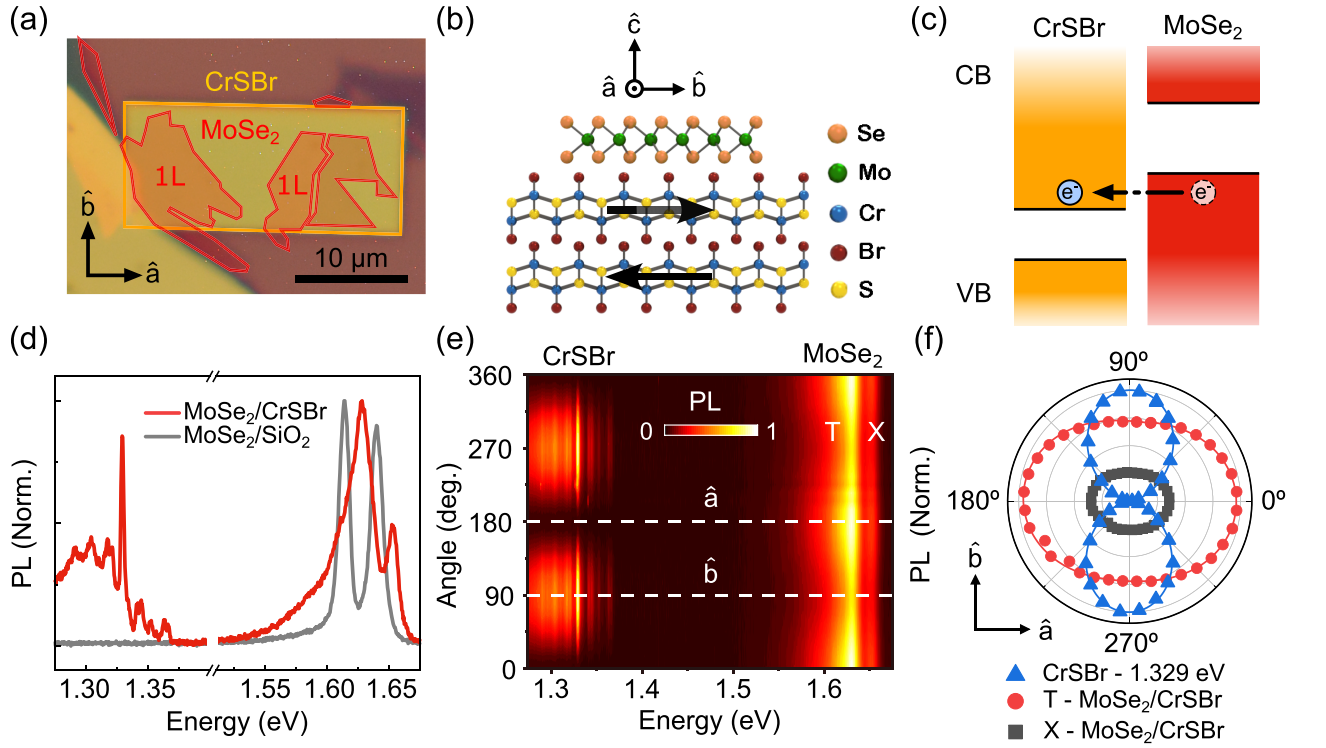

Figure 1. (a) Optical microscope image of the studied ML $MoSe_2$/bulk CrSBr vdW heterostructure, covered with a thin layer of hBN. The thickness of our CrSBr layer is about 35 nm (Figure S1). (b) Schematics of the crystal structure of the heterostructure. (c) Schematics of the band alignment of ML $MoSe_2$/bulk CrSBr and charge transfer from the $MoSe_2$ valence band (VB) to the CrSBr conduction band (CB). (d) Typical PL spectra from ML $MoSe_2$/CrSBr and $MoSe_2/SiO_2$ regions at 3.6 K. The laser energy is 1.88 eV. (e) Color-coded map of the linearly polarized emission intensity as a function of the angle of in-plane polarization. The laser excitation is linearly polarized along the $\hat{a}$ axis. (f) Polar plot of the PL intensity versus the in-plane linear polarization angle for the most intense PL peak energy of CrSBr (1.329 eV) and also for the exciton (X) and trion (T) emission peaks from $MoSe_2$ on CrSBr.

which is not well understood but might be related to crystal defects[26] or spin-freezing effects.[13] The CrSBr crystal consists of layers with rectangular unit cells in the plane ($\hat{a}$–$\hat{b}$) which are stacked along the $\hat{c}$ axis to produce an orthorhombic structure [Figure 1(b)]. The optical properties of CrSBr reflect its highly anisotropic electronic and magnetic structure. A prominent example is the coupling of excitons to magnetic order. Changes in the static magnetic configuration induced by applying a magnetic field, for instance, directly impact the exciton energy. The electronic band structure, and consequently the energy of excitons in CrSBr, are sensitive to the interlayer magnetic exchange interaction which can be used to probe its magnetic properties.[7,28,30,34]

Monolayer $MoSe_2$ is a direct band gap semiconductor with two inequivalent ±K valleys and robust excitons.[35−43] Under out-of-plane magnetic fields, valley Zeeman effects and magnetic-field-induced valley polarization are observed, and these effects depend on the presence of strain, doping, and magnetic proximity effects.[25,44−56]

Figure 1(a) shows an optical microscope image of our $MoSe_2$/CrSBr heterostructure and the crystal orientations, $\hat{a}$ and $\hat{b}$, of the CrSBr bulk crystal, while in Figure 1(b) the $MoSe_2$ and CrSBr crystal structures are sketched. Figure 1(c) presents the predicted type-III (broken-gap) band alignment of the heterostructure. In Figure 1(d), the PL spectrum of CrSBr at 3.6 K is displayed in the left part. Several PL peaks are observed below 1.4 eV and associated with excitons,[7,34,57,58] defects,[26] and strong exciton−photon coupling.[59]

Figure 1(d) shows the exciton and trion peaks in the normalized PL spectra of $MoSe_2$/CrSBr and $MoSe_2/SiO_2$. We observe a blue shift of the PL peaks and an important reduction of the PL intensity for $MoSe_2$/CrSBr compared to $MoSe_2/SiO_2$ (see Figure S2). It is important to mention that the predicted type-III band alignment results in an efficient interband charge transfer. Despite this, not all excited charge carriers are transferred as this effect depends on the interlayer band offset and quality of the interface. Therefore, the emission in $MoSe_2$/CrSBr is observed but with a reduced intensity. According to our theoretical predictions for the band alignment [see Figure 2(e,f)], the $MoSe_2$ layer may be strongly p-doped, while $MoSe_2$ on SiO_2 is usually n-doped.[47,52] Therefore, the trion in $MoSe_2$/CrSBr is most likely a positively charged exciton. In addition, we observe a low energy shoulder on the trion emission peak. We hypothesize that this shoulder may arise from trions localized at charged impurities[60] or relate to inelastic scattering of trions in $MoSe_2$ with magnons in CrSBr. Furthermore, we observe that the $MoSe_2$ trion PL peak has a significantly larger line width for $MoSe_2$/CrSBr as compared to $MoSe_2/SiO_2$. The reason behind such an increased PL line width is still unknown, suggesting that further studies are necessary to understand the observed result.

Next, we investigate the light-polarization properties in detail. The anisotropic optical emission of the CrSBr layer is evidenced by linear polarization-resolved PL measurements. Figure 1(e) shows a color map of the linearly polarized PL intensity as a function of the in-plane linear polarization angle at 3.6 K. The polar plots for these emissions are shown in

https://doi.org/10.1021/acs.nanolett.3c03431
Nano Lett. 2023, 23, 11073−11081

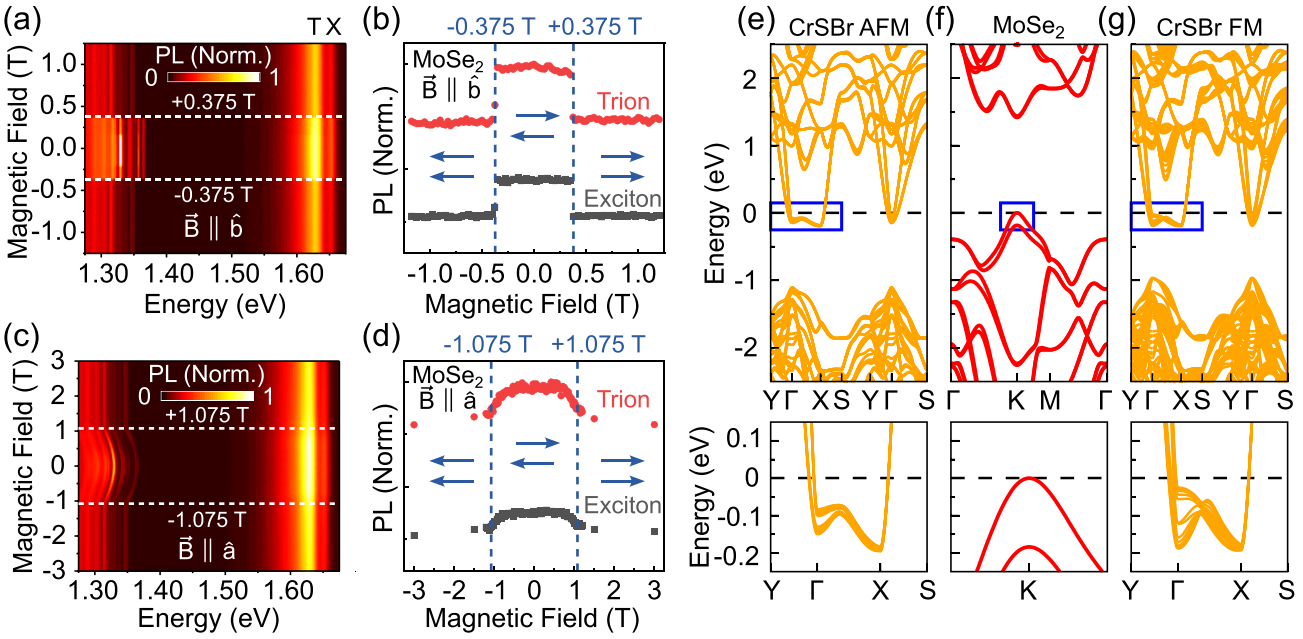

Figure 2. (a,c) Color-code map for circularly polarized PL intensity from the $MoSe_2$/CrSBr heterostructure as a function of the in-plane magnetic field, oriented along the in-plane easy (for $\vec{B} \parallel \hat{b}$) and intermediate axes (for $\vec{B} \parallel \hat{a}$). The excitation is performed using a linearly polarized laser. The PL detection is σ^- for positive magnetic fields. (b,d) Magnetic-field dependence of the $MoSe_2$ PL intensity of the exciton and trion emissions for both field orientations; the $MoSe_2$ PL intensity is sensitive to the magnetic phases of the CrSBr. Calculated band structure with spin−orbit coupling for (e) CrSBr AFM, (f) ML $MoSe_2$, and (g) CrSBr FM systems. The CrSBr systems consist of 6 layers. The horizontal dashed lines indicate the Fermi energy aligned with respect to the vacuum levels. The bottom panels show the band structure in the region of the blue rectangles, indicating clear differences of the AFM and FM energy levels next to the Fermi energy.

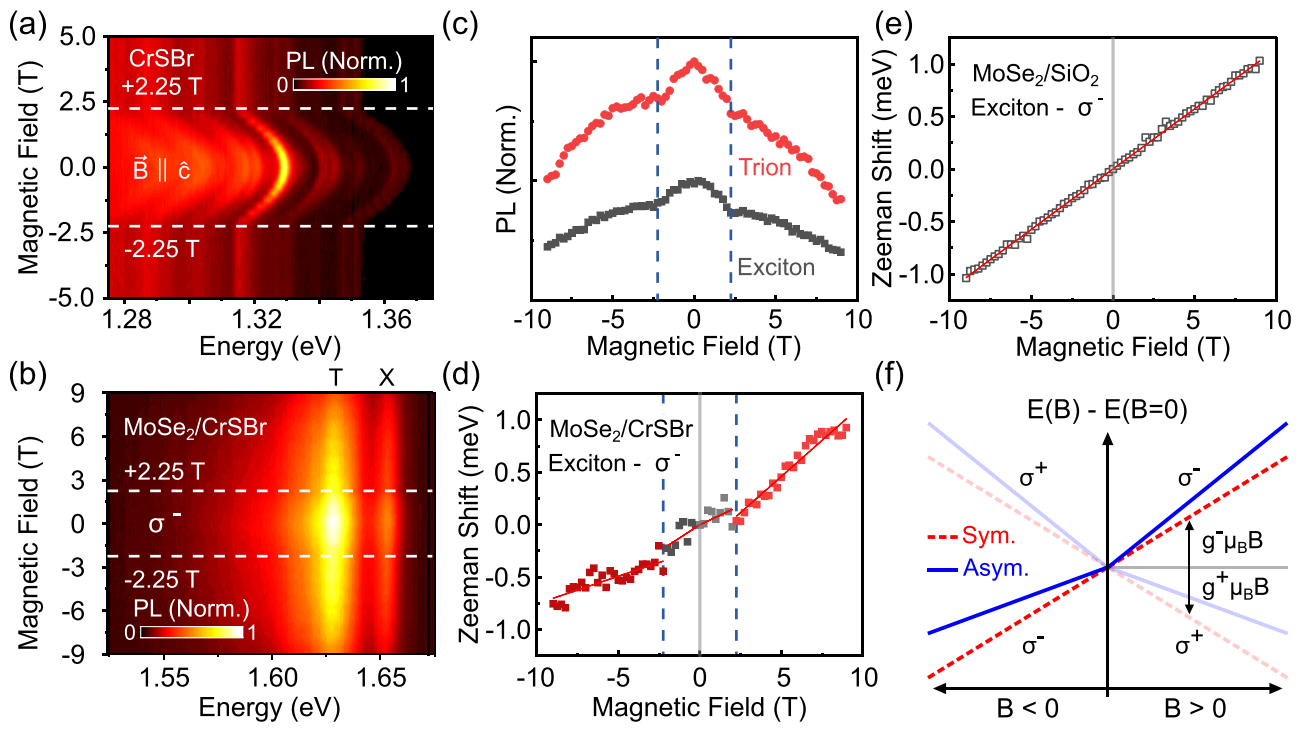

Figure 3. Color-code map of the circularly resolved PL intensity as a function of the out-of-plane magnetic field for (a) CrSBr and (b) $MoSe_2$/CrSBr. The laser excitation is linearly polarized, and the PL detection is σ^- for positive magnetic field. (c) PL intensity of exciton and trion peaks of $MoSe_2$/CrSBr as a function of magnetic field. Zeeman shift for the exciton peaks in the region of (d) $MoSe_2$/CrSBr and (e) $MoSe_2/SiO_2$. The solid lines are the fittings to the data. The extracted g-factors are summarized in Table 1. (f) Schematic representation of symmetric (dashed lines) and asymmetric (solid lines) Zeeman shifts as a function of magnetic field. The transparent lines indicate the σ^+ polarization that is not being measured.

Figure 1(f). All CrSBr PL peaks are strongly linearly polarized along the $\hat{b}$ axis, which shows the anisotropic electronic structure of CrSBr, as expected. Remarkably, a clear dependence of the PL intensity on the in-plane polarization angle is

https://doi.org/10.1021/acs.nanolett.3c03431
Nano Lett. 2023, 23, 11073−11081

observed for both the $MoSe_2$ exciton [black squares in Figure 1(f)] and trion [red circles in Figure 1(f)] emissions. This result indicates that $MoSe_2$ has acquired a linear-polarization component along the $\hat{a}$ axis probably due to magnetic proximity or photonic effects due to the linear dichroism of CrSBr.

We have also measured the PL for different magnetic field ($\vec{B}$) orientations. Figures 2(a) and (c) show color maps of the $MoSe_2$/CrSBr magneto-PL intensity under $\vec{B}$ parallel to the in-plane easy ($\vec{B} \parallel \hat{b}$) and hard axes ($\vec{B} \parallel \hat{a}$), respectively. For $\vec{B} \parallel \hat{b}$, the PL spectrum of CrSBr red-shifts abruptly by about 15 meV above a field of 0.375 T and is constant above 0.375 T (see also Figures S6 and S7). This result is similar to previous magneto-optical measurements for few-layer CrSBr[28] and was explained by a spin-flip transition from AFM to FM order also observed in magnetization measurements.[26] Under $\vec{B} \parallel \hat{a}$, the PL spectrum shifts smoothly, due to the canting of the spins along $\vec{B}$, saturating at B = 1.075 T beyond which the PL spectrum remains unchanged. The observed PL red shifts of CrSBr with increasing magnetic field were explained by a magnetization-dependent interlayer electronic coupling in the CrSBr material.[28]

Remarkably, we also find that the PL intensities of the $MoSe_2$ trion and exciton are correlated to the field-induced phase transition in CrSBr bulk: for $\vec{B} \parallel \hat{b}$ an abrupt change of the PL intensity of $MoSe_2$ above the critical magnetic field of 0.375 T occurs [see Figure 2(b) and Figures S6 and S7], and for $\vec{B} \parallel \hat{a}$, a continuous decrease of both $MoSe_2$ PL intensities is present up to 1.075 T, which corresponds to the saturation of the magnetization in CrSBr. Furthermore, the relative intensity of the trion/exciton peaks (Figure S8) also shows an abrupt change for $\vec{B} \parallel \hat{b}$, above the critical field of 0.375 T, and a continuous change up to 1.075 T for $\vec{B} \parallel \hat{a}$, which would indicate an increase in the doping of $MoSe_2$. This could be explained by a change of charge transfer after the magnetic-field-induced phase transition.

These results can be rationalized by our first-principles calculations of the electronic band structure shown in Figure 2(e−g). Not only the electronic structures of CrSBr in the AFM/FM phases are different[28,61] but also their band alignment (type-III) with respect to $MoSe_2$ changes [see bottom panels in Figures 2(e−g)]. These energetic differences suggest that the charge transfer between ML $MoSe_2$ and CrSBr can be drastically altered when increasing the magnetic field because of the transition from AFM to FM phases in CrSBr.

Let us now turn to the magneto-PL investigations of the $MoSe_2$/CrSBr heterostructure for an out-of-plane magnetic field ($\vec{B} \parallel \hat{c}$) under linearly polarized excitation and σ^- circularly polarized PL detection as a function of $\vec{B}$. For CrSBr emission energies [Figure 3(a)], a continuous red-shift of all PL peaks occurs while increasing B (in absolute value) up to a saturation field of about 2.25 T, beyond which the PL peaks remains unchanged, consistent with previous reports.[28] For $MoSe_2$, the color code map of PL intensity as a function of B is shown in Figure 3(b). It also exhibits a correlation with the magnetic phase order of CrSBr. Figure 3(c) presents the intensities of the exciton and trion PL peaks as a function of B. We observe an unusual change of the PL intensity for both exciton and trion, in the range of −2.25 to +2.25 T, which is correlated to the magnetic-field-induced phase transition of CrSBr. In addition, we observe a blue (red) shift of PL peak positions as shown in Figure 3(b) and (d) with an increase of positive (negative) B values, resembling the effects of the valley Zeeman splitting.[47,48]

The B dependence for one particular polarization branch (σ^+ or σ^-) of the PL peak of the exciton or trion in TMDs can be written as[50,62,63]

$$E_i(B) = E_i(B = 0) + g_i^j \mu_B B \tag{1}$$

in which μ_B is the Bohr magneton, the subindex $i = X(T)$ identifies the exciton (trion), and the superindex $j = \pm$ denotes the circular polarization $\sigma^{\pm}$. Equation 1 describes the Zeeman shift of one polarization branch (the increase or decrease depends on the sign of g_i^j, which is system dependent), whereas the Zeeman splitting requires knowledge of the Zeeman shifts for each polarization. The total g-factor that modulates the Zeeman splitting is then given by $g_i = g_i^+ - g_i^-$. In pristine monolayer TMDs, $g_X^+ \sim -2$ and $g_X^- \sim 2$ (directly related to the angular momenta of the valence and conduction band states at the K valleys involved in the exciton transition[53,64]), leading to a total g-factor of $g_X \sim -4$. Furthermore, time reversal symmetry connects the g-factors obtained at positive and negative magnetic fields via $g_i^+(B > 0) = -g_i^-(B < 0)$, allowing us to recover the Zeeman shift of the σ^+ branch by measuring the σ^- branch at negative magnetic fields.

The excitonic Zeeman shift obtained for the $MoSe_2$/CrSBr heterostructure is displayed in Figure 3(d). As a reference, we have also measured the magneto-PL in the $MoSe_2/SiO_2$ region of the sample [see Figure 3(e)]. The Zeeman shifts of the trion peaks are presented in Figure S10 and closely follow the excitonic features. Our results reveal an intriguing asymmetric signature in the Zeeman shift of the $MoSe_2$ exciton within the $MoSe_2$/CrSBr heterostructure, while the $MoSe_2/SiO_2$ system displays a symmetric response. The observed change of g-factors for AFM and FM orders (see Table 1) cannot be related to doping effects[63,65] since the trion/exciton intensity ratio shows only a small variation with respect to the magnetic field (see Figure S8). More importantly, doping effects do not account for the observed Zeeman shift asymmetry. These findings point to an asymmetric coupling between the $MoSe_2$ valleys and the CrSBr bands, which is dependent on magnetic ordering. Exploiting time reversal symmetry allows us to extract distinct g_i^+ and g_i^- values for each magnetic phase at positive and negative magnetic fields. In Figure 3(f), we present a schematic representation of the symmetric and asymmetric Zeeman shifts, summarizing the observed features of Figures 3(d,e). The obtained g-factors for excitons and

Table 1. Exciton and Trion g-Factors for $B > 0$[a]

			$MoSe_2$/CrSBr	
		$MoSe_2/SiO_2$	AFM	FM
Exciton	g_X^+	−1.98 ± 0.05	−1.75 ± 0.39	−0.90 ± 0.05
	g_X^-	1.97 ± 0.05	1.25 ± 0.44	2.37 ± 0.05
	g_X	−4.0 ± 0.1	−3.0 ± 0.8	−3.3 ± 0.1
Trion	g_T^+	−2.10 ± 0.05	−1.33 ± 0.18	−1.42 ± 0.06
	g_T^-	2.14 ± 0.05	2.25 ± 0.46	1.84 ± 0.06
	g_T	−4.2 ± 0.1	−3.6 ± 0.6	−3.3 ± 0.1

[a]The g-factors for σ^+ were obtained via $g_i^+ = -g_i^-(B < 0)$, and the total g-factor is given by $g_i = g_i^+ - g_i^-$. In the AFM phase, assisted by small fields, the Zeeman shifts approach the spectral resolution of the system, resulting in higher error bars for the obtained values. Nevertheless, the errors are still smaller than the extracted g-factors and allow us to unambiguously identify the asymmetric signatures.

https://doi.org/10.1021/acs.nanolett.3c03431
Nano Lett. 2023, 23, 11073−11081

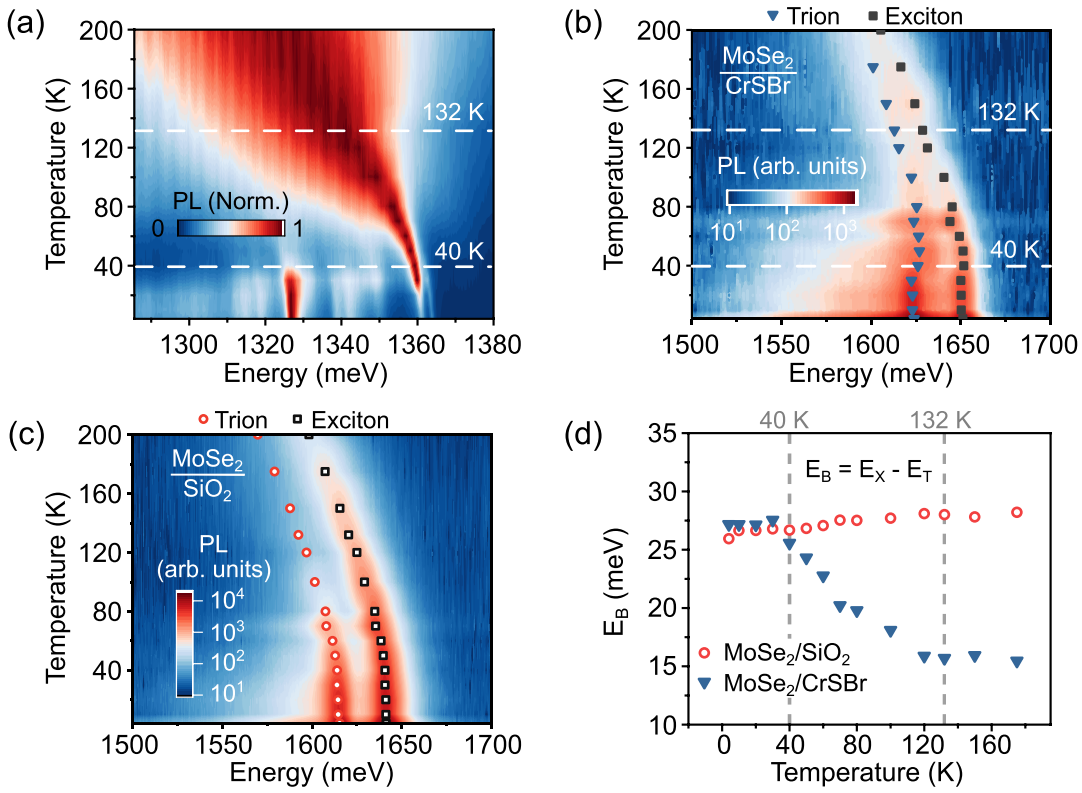

Figure 4. (a) Color-code map of PL intensity as a function of temperature for the PL peaks of the CrSBr. The highest dot-dashed line indicates the CrSBr Néel temperature transition at 132 K, and the lower one at 40 K indicates the temperature where sharpening of the peaks appears. (b,c) Color-code maps of the PL intensity as a function of the temperature for the exciton and trion peaks from (b) $MoSe_2$/CrSBr and (c) $MoSe_2/SiO_2$. (d) Trion binding energy extracted from the data shown in (c) and (d).

trions are summarized in Table 1. Particularly, for the excitons in $MoSe_2/SiO_2$, we extract $|g^+_{X,T}| = |g^-_{X,T}|$, leading to a total *g*-factor of ∼−4.0, consistent with theoretical[53,54,64,66] and experimental values, reported in the literature for $MoSe_2/SiO_2$ or hBN/$MoSe_2$/hBN.[42,45,47,48,52,67−71] For the $MoSe_2$ excitons on CrSBr, $|g^+_{X,T}|$ is distinctly different from $|g^-_{X,T}|$, and the total *g*-factor is less negative than the typical values of −4 in pristine $MoSe_2$. Our study uncovers notable variations in the *g*-factors of the $MoSe_2$ exciton and trion when CrSBr undergoes transitions between the AFM and FM phases, revealing an asymmetric coupling between the spin−valley properties of $MoSe_2$ and the magnetic ordering of CrSBr. These distinct *g*-factors provide valuable insights into the intricate interplay between electronic and magnetic degrees of freedom, underscoring the importance of considering the magnetic state of CrSBr in understanding the behavior of excitonic systems in this heterostructure. The changes in the magnitude of the *g*-factors are consistent with proximity effects due to the hybridization between the layers, as previously demonstrated in $MoSe_2/WSe_2$,[53,72] WSe_2/CrI_3,[73] and WS_2/graphene systems.[74] A systematic analysis of the microscopic features behind the asymmetric *g*-factors is beyond the scope of the current manuscript; however, we point out that asymmetric signatures in valley Zeeman splitting have recently been observed in $MoSe_2/CrBr_3$[16] heterostructures at zero magnetic field. In these systems, the magnetic moments in $CrBr_3$ point in the out-of-plane direction and act already as an external magnetic field. Here, the magnetic moments of CrSBr are oriented in-plane, and therefore the asymmetric coupling is manifested once we apply an external magnetic field. The asymmetric Zeeman shifts do not necessarily require a magnetic material but can also be present in systems where valence bands are mixed.[75]

Furthermore, we have also measured the linear polarization of the PL of the heterostructure [see Figure S4(f)]. We find that the angle dependence and relative intensity of the trion/exciton of the $MoSe_2$ PL are clearly modified as compared to 0 T. The observed anisotropy of the relative intensities of the $MoSe_2$ trion/exciton could be explained by an anisotropic band structure of the heterostructure due to proximity effects.

We now analyze the temperature dependence of the PL data, shown in Figure 4. For CrSBr, a blue shift of the PL band is observed with a decrease in temperature, which is accompanied by a change in the peak shape around the magnetic phase transition (T_N around 132 K). In addition, at 40 K, sharp peaks appear below 1360 meV, together with a clear enhancement of the PL intensity of the peak at around 1330 meV. A clear correlation between the emission peaks and phase transitions in CrSBr is thus present.

Important changes are also observed for the PL of $MoSe_2$. At higher temperatures (T_N > 132 K), the trion binding energy of $MoSe_2$/CrSBr is much lower than that of $MoSe_2/SiO_2$, probably due to different dielectric constant values of CrSBr and SiO_2. Remarkably, we find an anomalous temperature dependence of the exciton and trion peak positions for $MoSe_2$/CrSBr. This is visualized in Figure 4(d) (see also Figures S11 and S12), where we plot the extracted trion binding energies versus temperature. The $MoSe_2$/CrSBr trion binding energy increases with decreasing temperature between the magnetic phase transitions, while it stabilizes above T_N and below 40 K.

https://doi.org/10.1021/acs.nanolett.3c03431
Nano Lett. 2023, 23, 11073−11081

A similar anomaly was observed in the temperature dependence of excitons in the $MoSe_2/MnPSe_3$ heterostructure near T_N and was associated with a coupling of $MoSe_2$ excitons to magnons in $MnPSe_3$.[3] In our heterostructure, $MoSe_2$ excitons may also couple to the (incoherent) magnons[57] of CrSBr at nonzero temperatures. The impact of these magnons on the CrSBr band structure has not yet been studied in detail, but it is expected that magnon-induced changes will affect both the charge transfer between $MoSe_2$ and CrSBr as well as the dielectric screening experienced by the excitons in $MoSe_2$. Both phenomena may contribute to the exciton/trion temperature dependence.[76−79] However, further studies will be necessary to understand in more detail this experimental result.

In summary, we have measured the linearly and circularly polarized PL on $MoSe_2$/CrSBr heterostructures under magnetic fields up to 9 T oriented along the different crystallographic axes of CrSBr. The results show that the valley and excitonic properties (intensity, energy position, and *g*-factors) of monolayer $MoSe_2$ are strongly influenced by the magnetic order of a CrSBr substrate. For all magnetic field orientations, we found that the $MoSe_2$ PL intensity is sensitive to the magnetic ordering of the CrSBr. We predict a type-III band alignment for $MoSe_2$/CrSBr which can account for the observed correlation of $MoSe_2$ PL intensity with the magnetic-induced phase transition of CrSBr. For out-of-plane magnetic fields, a clear asymmetric Zeeman shift is observed for $MoSe_2$/CrSBr. Furthermore, we observe an anomalous behavior of the trion binding energy as a function of temperature. The binding energy is considerably low at high temperatures and increases below T_N. In general, our results are explained by asymmetric magnetic proximity, charge transfer, exciton/trion magnon coupling, and dielectric anomalies of the 2D antiferromagnetic material. Our findings offer a unique insight into the interplay of proximity effects and charge transfer in antiferromagnetic−nonmagnetic interfaces that modify the exciton and valley properties of 2D TMDs.

■ ASSOCIATED CONTENT

Supporting Information

The Supporting Information is available free of charge at https://pubs.acs.org/doi/10.1021/acs.nanolett.3c03431.

Sample preparation, experimental methods and complementary PL results, and details on the first-principles calculations (PDF)

■ AUTHOR INFORMATION

Corresponding Author

Yara Galvão Gobato − *Physics Department, Federal University of São Carlos, São Carlos, SP 13565-905, Brazil;* orcid.org/0000-0003-2251-0426; Email: yara@df.ufscar.br

Authors

Caique Serati de Brito − *Physics Department, Federal University of São Carlos, São Carlos, SP 13565-905, Brazil; Institut für Experimentelle und Angewandte Physik, Universität Regensburg, D-93040 Regensburg, Germany;* orcid.org/0000-0003-3992-1731

Paulo E. Faria Junior − *Institute for Theoretical Physics, University of Regensburg, D-93040 Regensburg, Germany*

Talieh S. Ghiasi − *Kavli Institute of Nanoscience, Delft University of Technology, 2628 CJ Delft, The Netherlands;* orcid.org/0000-0002-3490-5356

Josep Ingla-Aynés − *Kavli Institute of Nanoscience, Delft University of Technology, 2628 CJ Delft, The Netherlands;* orcid.org/0000-0001-9179-1570

César Ricardo Rabahi − *Physics Department, Federal University of São Carlos, São Carlos, SP 13565-905, Brazil;* orcid.org/0000-0002-9054-4997

Camila Cavalini − *Physics Department, Federal University of São Carlos, São Carlos, SP 13565-905, Brazil*

Florian Dirnberger − *Institute of Applied Physics and Würzburg-Dresden Cluster of Excellence ct.qmat, Technische Universität, 01069 Dresden, Germany*

Samuel Mañas-Valero − *Kavli Institute of Nanoscience, Delft University of Technology, 2628 CJ Delft, The Netherlands; Instituto de Ciencia Molecular (ICMol), Universitat de València, Paterna 46980, Spain;* orcid.org/0000-0001-6319-9238

Kenji Watanabe − *Research Center for Materials Nanoarchitectonics, National Institute for Materials Science, Tsukuba 305-0044, Japan;* orcid.org/0000-0003-3701-8119

Takashi Taniguchi − *Research Center for Materials Nanoarchitectonics, National Institute for Materials Science, Tsukuba 305-0044, Japan;* orcid.org/0000-0002-1467-3105

Klaus Zollner − *Institute for Theoretical Physics, University of Regensburg, D-93040 Regensburg, Germany*

Jaroslav Fabian − *Institute for Theoretical Physics, University of Regensburg, D-93040 Regensburg, Germany*

Christian Schüller − *Institut für Experimentelle und Angewandte Physik, Universität Regensburg, D-93040 Regensburg, Germany*

Herre S. J. van der Zant − *Kavli Institute of Nanoscience, Delft University of Technology, 2628 CJ Delft, The Netherlands;* orcid.org/0000-0002-5385-0282

Complete contact information is available at: https://pubs.acs.org/10.1021/acs.nanolett.3c03431

Notes

The authors declare no competing financial interest.

■ ACKNOWLEDGMENTS

This work was supported by Fundação de Amparo a Pesquisa do Estado de São Paulo (FAPESP) (grants 14/19142-1, 22/08329-0, and 23/01313-4) and by the Brazilian Council for Research (CNPq) (grant 311678/2020-3). C.S.B. acknowledges the financial support of CAPES fellowship. T.S.G. and H.vdZ. received funding from European Union Horizon 2020 research and innovation program under grant agreement No. 863098 (SPRING). P.E.F.J., K.Z., C.S., and J.F. acknowledge the financial support of the Deutsche Forschungsgemeinschaft (DFG, German Research Foundation) SFB 1277 (Project-ID 314695032, projects B05, B07, and B11), and SPP 2244 (Project No. 443416183, SCHU1171/10) and of the European Union Horizon 2020 Research and Innovation Program under Contract No. 881603 (Graphene Flagship). Y.G.G. and H.vdZ. acknowledge support from the Fapesp-SPRINT project (grant 22/00419-0). K.W. and T.T. acknowledge support from the JSPS KAKENHI (Grant Numbers 21H05233 and 23H02052) and World Premier International Research Center

Initiative (WPI), MEXT, Japan. S.M.-V. acknowledges the European Commission for a Marie Sklodowska−Curie individual fellowship No. 101103355 - SPIN-2D-LIGHT. J.I.A. acknowledges support from the European Union's Horizon 2020 research and innovation programme for a Marie Sklodowska−Curie individual fellowship No. 101027187-PCSV. F.D. acknowledges financial support from Alexey Chernikov and the Würzburg-Dresden Cluster of Excellence on Complexity and Topology in Quantum Matter ct.qmat (EXC 2147, Project-ID 390858490).

REFERENCES

(1) Lyons, T. P.; Gillard, D.; Molina-Sánchez, A.; Misra, A.; Withers, F.; Keatley, P. S.; Kozikov, A.; Taniguchi, T.; Watanabe, K.; Novoselov, K. S.; Fernández-Rossier, J.; Tartakovskii, A. I. Interplay between spin proximity effect and charge-dependent exciton dynamics in MoSe2/CrBr3 van der Waals heterostructures. *Nat. Commun.* **2020**, *11*, 1−9.

(2) Zhong, D.; Seyler, K. L.; Linpeng, X.; Wilson, N. P.; Taniguchi, T.; Watanabe, K.; McGuire, M. A.; Fu, K. M. C.; Xiao, D.; Yao, W.; Xu, X. Layer-resolved magnetic proximity effect in van der Waals heterostructures. *Nat. Nanotechnol.* **2020**, *15*, 187−191.

(3) Onga, M.; Onga, M.; Sugita, Y.; Ideue, T.; Nakagawa, Y.; Nakagawa, Y.; Suzuki, R.; Suzuki, R.; Motome, Y.; Iwasa, Y.; Iwasa, Y.; Iwasa, Y. Antiferromagnet-Semiconductor Van der Waals Heterostructures: Interlayer Interplay of Exciton with Magnetic Ordering. *Nano Lett.* **2020**, *20*, 4625−4630.

(4) Li, Y.; Yang, B.; Xu, S.; Huang, B.; Duan, W. Emergent Phenomena in Magnetic Two-Dimensional Materials and van der Waals Heterostructures. *ACS Appl. Electron. Mater.* **2022**, *4*, 3278−3302.

(5) Choi, E.-M.; Sim, K. I.; Burch, K. S.; Lee, Y. H.; Choi, E.-M.; Sim, K. I.; Lee, Y. H.; Burch, K. S. Emergent Multifunctional Magnetic Proximity in van der Waals Layered Heterostructures. *Advanced Science* **2022**, *9*, 2200186.

(6) Seyler, K. L.; Zhong, D.; Huang, B.; Linpeng, X.; Wilson, N. P.; Taniguchi, T.; Watanabe, K.; Yao, W.; Xiao, D.; McGuire, M. A.; Fu, K. M. C.; Xu, X. Valley Manipulation by Optically Tuning the Magnetic Proximity Effect in WSe2/CrI3 Heterostructures. *Nano Lett.* **2018**, *18*, 3823−3828.

(7) Pawbake, A.; et al. Magneto-Optical Sensing of the Pressure Driven Magnetic Ground States in Bulk CrSBr. *Nano Lett.* **2023**, *23*, 9587−9593.

(8) Scharf, B.; Xu, G.; Matos-Abiague, A.; Žutić, I. Magnetic Proximity Effects in Transition-Metal Dichalcogenides: Converting Excitons. *Phys. Rev. Lett.* **2017**, *119*, 127403.

(9) Huang, B.; Clark, G.; Navarro-Moratalla, E.; Klein, D. R.; Cheng, R.; Seyler, K. L.; Zhong, D.; Schmidgall, E.; McGuire, M. A.; Cobden, D. H.; Yao, W.; Xiao, D.; Jarillo-Herrero, P.; Xu, X. Layer-dependent ferromagnetism in a van der Waals crystal down to the monolayer limit. *Nature* **2017**, *546*, 270−273.

(10) Zhang, Z.; Ni, X.; Huang, H.; Hu, L.; Liu, F. Valley splitting in the van der Waals heterostructure WSe2/CrI3: The role of atom superposition. *Phys. Rev. B* **2019**, *99*, 115441.

(11) Xie, J.; Jia, L.; Shi, H.; Yang, D.; Si, M. Electric field mediated large valley splitting in the van der Waals heterostructure WSe2/CrI3. *Jpn. J. Appl. Phys.* **2019**, *58*, No. 010906.

(12) Ahn, E. C. 2D materials for spintronic devices. *npj 2D Mater. Appl.* **2020**, *4*, 1−14.

(13) Boix-Constant, C.; et al. Probing the Spin Dimensionality in Single-Layer CrSBr Van Der Waals Heterostructures by Magneto-Transport Measurements. *Adv. Mater.* **2022**, *34*, 2204940.

(14) Geim, A. K.; Grigorieva, I. V. Van der Waals heterostructures. *Nature* **2013**, *499*, 419−425.

(15) Novoselov, K. S.; Mishchenko, A.; Carvalho, A.; Castro Neto, A. H. 2D materials and van der Waals heterostructures. *Science* **2016**, *353*, aac9439.

(16) Choi, J.; Lane, C.; Zhu, J. X.; Crooker, S. A. Asymmetric magnetic proximity interactions in MoSe2/CrBr3 van der Waals heterostructures. *Nat. Mater.* **2023**, *22*, 305−310.

(17) Zhong, D.; Seyler, K. L.; Linpeng, X.; Cheng, R.; Sivadas, N.; Huang, B.; Schmidgall, E.; Taniguchi, T.; Watanabe, K.; McGuire, M. A.; Yao, W.; Xiao, D.; Fu, K. M. C.; Xu, X. Van der Waals engineering of ferromagnetic semiconductor heterostructures for spin and valleytronics. *Science Advances* **2017**, *3*, e1603113.

(18) Huang, B.; McGuire, M. A.; May, A. F.; Xiao, D.; Jarillo-Herrero, P.; Xu, X. Emergent phenomena and proximity effects in two-dimensional magnets and heterostructures. *Nat. Mater.* **2020**, *19*, 1276−1289.

(19) Mak, K. F.; Shan, J.; Ralph, D. C. Probing and controlling magnetic states in 2D layered magnetic materials. *Nature Reviews Physics* **2019**, *1*, 646−661.

(20) Zollner, K.; Faria Junior, P. E.; Fabian, J. Proximity exchange effects in MoSe2 and WSe2 heterostructures with CrI3: Twist angle, layer, and gate dependence. *Phys. Rev. B* **2019**, *100*, No. 085128.

(21) Zollner, K.; Faria Junior, P. E.; Fabian, J. Giant proximity exchange and valley splitting in transition metal dichalcogenide/hBN/(Co, Ni) heterostructures. *Phys. Rev. B* **2020**, *101*, No. 085112.

(22) Zollner, K.; Faria Junior, P. E.; Fabian, J. Strong manipulation of the valley splitting upon twisting and gating in $MoSe_2$ /CrI_3 and WSe_2 /CrI_3 van der Waals heterostructures. *Phys. Rev. B* **2023**, *107*, No. 035112.

(23) Zhao, C.; et al. Enhanced valley splitting in monolayer WSe2 due to magnetic exchange field. *Nat. Nanotechnol.* **2017**, *12*, 757−762.

(24) Norden, T.; Zhao, C.; Zhang, P.; Sabirianov, R.; Petrou, A.; Zeng, H. Giant valley splitting in monolayer WS2 by magnetic proximity effect. *Nat. Commun.* **2019**, *10*, 1−10.

(25) Ciorciaro, L.; Kroner, M.; Watanabe, K.; Taniguchi, T.; Imamoglu, A. Observation of Magnetic Proximity Effect Using Resonant Optical Spectroscopy of an Electrically Tunable MoSe2/CrBr3 Heterostructure. *Phys. Rev. Lett.* **2020**, *124*, 197401.

(26) Klein, J.; et al. Sensing the Local Magnetic Environment through Optically Active Defects in a Layered Magnetic Semiconductor. *ACS Nano* **2023**, *17*, 288−299.

(27) Lee, K.; Dismukes, A. H.; Telford, E. J.; Wiscons, R. A.; Wang, J.; Xu, X.; Nuckolls, C.; Dean, C. R.; Roy, X.; Zhu, X. Magnetic Order and Symmetry in the 2D Semiconductor CrSBr. *Nano Lett.* **2021**, *21*, 3511−3517.

(28) Wilson, N. P.; Lee, K.; Cenker, J.; Xie, K.; Dismukes, A. H.; Telford, E. J.; Fonseca, J.; Sivakumar, S.; Dean, C.; Cao, T.; Roy, X.; Xu, X.; Zhu, X. Interlayer electronic coupling on demand in a 2D magnetic semiconductor. *Nat. Mater.* **2021**, *20*, 1657−1662.

(29) Telford, E. J.; et al. Coupling between magnetic order and charge transport in a two-dimensional magnetic semiconductor. *Nat. Mater.* **2022**, *21*, 754−760.

(30) López-Paz, S. A.; Guguchia, Z.; Pomjakushin, V. Y.; Witteveen, C.; Cervellino, A.; Luetkens, H.; Casati, N.; Morpurgo, A. F.; von Rohr, F. O. Dynamic magnetic crossover at the origin of the hidden-order in van der Waals antiferromagnet CrSBr. *Nat. Commun.* **2022**, *13*, 1−10.

(31) Ye, C.; Wang, C.; Wu, Q.; Liu, S.; Zhou, J.; Wang, G.; Soll, A.; Sofer, Z.; Yue, M.; Liu, X.; Tian, M.; Xiong, Q.; Ji, W.; Renshaw Wang, X. Layer-Dependent Interlayer Antiferromagnetic Spin Reorientation in Air-Stable Semiconductor CrSBr. *ACS Nano* **2022**, *16*, 11876−11883.

(32) Ghiasi, T. S.; Kaverzin, A. A.; Dismukes, A. H.; de Wal, D. K.; Roy, X.; van Wees, B. J. Electrical and thermal generation of spin currents by magnetic bilayer graphene. *Nat. Nanotechnol.* **2021**, *16*, 788−794.

(33) Bae, Y. J.; et al. Exciton-coupled coherent magnons in a 2D semiconductor. *Nature* **2022**, *609*, 282−286.

(34) Klein, J.; et al. The Bulk van der Waals Layered Magnet CrSBr is a Quasi-1D Material. *ACS Nano* **2023**, *17*, 5316−5328.

(35) Mak, K. F.; Lee, C.; Hone, J.; Shan, J.; Heinz, T. F. Atomically thin MoS2: A new direct-gap semiconductor. *Phys. Rev. Lett.* **2010**, *105*, 136805.

https://doi.org/10.1021/acs.nanolett.3c03431
Nano Lett. 2023, 23, 11073−11081

(36) Splendiani, A.; Sun, L.; Zhang, Y.; Li, T.; Kim, J.; Chim, C. Y.; Galli, G.; Wang, F. Emerging photoluminescence in monolayer MoS2. *Nano Lett.* **2010**, *10*, 1271−1275.
(37) Xu, X.; Yao, W.; Xiao, D.; Heinz, T. F. Spin and pseudospins in layered transition metal dichalcogenides. *Nat. Phys.* **2014**, *10*, 343−350.
(38) Xiao, D.; Liu, G. B.; Feng, W.; Xu, X.; Yao, W. Coupled spin and valley physics in monolayers of MoS 2 and other group-VI dichalcogenides. *Phys. Rev. Lett.* **2012**, *108*, 196802.
(39) Mak, K. F.; He, K.; Shan, J.; Heinz, T. F. Control of valley polarization in monolayer MoS2 by optical helicity. *Nat. Nanotechnol.* **2012**, *7*, 494−498.
(40) Zeng, H.; Dai, J.; Yao, W.; Xiao, D.; Cui, X. Valley polarization in MoS2 monolayers by optical pumping. *Nat. Nanotechnol.* **2012**, *7*, 490−493.
(41) Schaibley, J. R.; Yu, H.; Clark, G.; Rivera, P.; Ross, J. S.; Seyler, K. L.; Yao, W.; Xu, X. Valleytronics in 2D materials. *Nat. Rev. Mater.* **2016**, *1*, 1−15.
(42) Gobato, Y. G.; Brito, C. S. D.; Chaves, A.; Prosnikov, M. A.; Woźniak, T.; Guo, S.; Barcelos, I. D.; Milošević, M. V.; Withers, F.; Christianen, P. C. Distinctive g-Factor of Moiré-Confined Excitons in van der Waals Heterostructures. *Nano Lett.* **2022**, *22*, 8641−8646.
(43) Ishii, S.; Yokoshi, N.; Ishihara, H. Optical selection rule of monolayer transition metal dichalcogenide by an optical vortex. *Journal of Physics: Conference Series* **2019**, *1220*, No. 012056.
(44) Aivazian, G.; Gong, Z.; Jones, A. M.; Chu, R. L.; Yan, J.; Mandrus, D. G.; Zhang, C.; Cobden, D.; Yao, W.; Xu, X. Magnetic control of valley pseudospin in monolayer WSe2. *Nat. Phys.* **2015**, *11*, 148−152.
(45) Li, Y.; Ludwig, J.; Low, T.; Chernikov, A.; Cui, X.; Arefe, G.; Kim, Y. D.; van der Zande, A. M.; Rigosi, A.; Hill, H. M.; Kim, S. H.; Hone, J.; Li, Z.; Smirnov, D.; Heinz, T. F. Valley splitting and polarization by the zeeman effect in monolayer MoSe2. *Phys. Rev. Lett.* **2014**, *113*, 266804.
(46) Srivastava, A.; Sidler, M.; Allain, A. V.; Lembke, D. S.; Kis, A.; Imamoglu, A. Valley Zeeman effect in elementary optical excitations of monolayer WSe2. *Nat. Phys.* **2015**, *11*, 141−147.
(47) Macneill, D.; Heikes, C.; Mak, K. F.; Anderson, Z.; Kormányos, A.; Zólyomi, V.; Park, J.; Ralph, D. C. Breaking of valley degeneracy by magnetic field in monolayer MoSe2. *Phys. Rev. Lett.* **2015**, *114*, No. 037401.
(48) Wang, G.; Bouet, L.; Glazov, M. M.; Amand, T.; Ivchenko, E. L.; Palleau, E.; Marie, X.; Urbaszek, B. Magneto-optics in transition metal diselenide monolayers. *2D Materials* **2015**, *2*, No. 034002.
(49) Mitioglu, A. A.; Plochocka, P.; Granados del Aguila, A.; Christianen, P. C. M.; Deligeorgis, G.; Anghel, S.; Kulyuk, L.; Maude, D. K. Optical Investigation of Monolayer and Bulk Tungsten Diselenide (WSe2) in High Magnetic Fields. *Nano Lett.* **2015**, *15*, 4387−4392.
(50) Stier, A. V.; McCreary, K. M.; Jonker, B. T.; Kono, J.; Crooker, S. A. Exciton diamagnetic shifts and valley Zeeman effects in monolayer WS2 and MoS2 to 65 T. *Nat. Commun.* **2016**, *7*, 1−8.
(51) Plechinger, G.; Nagler, P.; Arora, A.; Granados del Aguila, A.; Ballottin, M. V.; Frank, T.; Steinleitner, P.; Gmitra, M.; Fabian, J.; Christianen, P. C. M.; Bratschitsch, R.; Schuller, C.; Korn, T. Excitonic Valley Effects in Monolayer WS2 under High Magnetic Fields. *Nano Lett.* **2016**, *16*, 7899−7904.
(52) Covre, F. S.; Faria Junior, P. E.; Gordo, V. O.; de Brito, C. S.; Zhumagulov, Y. V.; Teodoro, M. D.; Couto, O. D.; Misoguti, L.; Pratavieira, S.; Andrade, M. B.; Christianen, P. C.; Fabian, J.; Withers, F.; Gobato, Y. G. Revealing the impact of strain in the optical properties of bubbles in monolayer MoSe2. *Nanoscale* **2022**, *14*, 5758−5768.
(53) Woźniak, T.; Faria Junior, P. E.; Seifert, G.; Chaves, A.; Kunstmann, J. Exciton g factors of van der Waals heterostructures from first-principles calculations. *Phys. Rev. B* **2020**, *101*, 235408.
(54) Deilmann, T.; Krüger, P.; Rohlfing, M. Ab Initio Studies of Exciton *g*Factors: Monolayer Transition Metal Dichalcogenides in Magnetic Fields. *Phys. Rev. Lett.* **2020**, *124*, 226402.
(55) Xuan, F.; Quek, S. Y. Valley-filling instability and critical magnetic field for interaction-enhanced Zeeman response in doped WSe2 monolayers. *npj Computational Materials* **2021**, *7*, 198.
(56) Back, P.; Sidler, M.; Cotlet, O.; Srivastava, A.; Takemura, N.; Kroner, M.; Imamoğlu, A. Giant Paramagnetism-Induced Valley Polarization of Electrons in Charge-Tunable Monolayer MoSe2. *Phys. Rev. Lett.* **2017**, *118*, 237404.
(57) Dirnberger, F.; Quan, J.; Bushati, R.; Diederich, G. M.; Florian, M.; Klein, J.; Mosina, K.; Sofer, Z.; Xu, X.; Kamra, A.; García-Vidal, F. J.; Alù, A.; Menon, V. M. Magneto-optics in a van der Waals magnet tuned by self-hybridized polaritons. *Nature* **2023**, *620*, 533−537.
(58) Marques-Moros, F.; Boix-Constant, C.; Mañas-Valero, S.; Canet-Ferrer, J.; Coronado, E. Interplay between Optical Emission and Magnetism in the van der Waals Magnetic Semiconductor CrSBr in the Two-Dimensional Limit. *ACS Nano* **2023**, *17*, 13224−13231.
(59) Lin, K.; Sun, X.; Dirnberger, F.; Li, Y.; Qu, J.; Wen, P.; Sofer, Z.; Söll, A.; Winnerl, S.; Helm, M.; Zhou, S.; Dan, Y.; Prucnal, S. Strong Exciton-Phonon Coupling as a Fingerprint of Magnetic Ordering in van der Waals Layered CrSBr. *arXiv preprint arXiv:2308.04895 [cond-mat.mtrl-sci]* **2023** (accessed 2023-11-15).
(60) Schwemmer, M.; Nagler, P.; Hanninger, A.; Schüller, C.; Korn, T. Long-lived spin polarization in n-doped $MoSe_2$ monolayers. *Appl. Phys. Lett.* **2017**, *111*, No. 082404.
(61) Bianchi, M.; Acharya, S.; Dirnberger, F.; Klein, J.; Pashov, D.; Mosina, K.; Sofer, Z.; Rudenko, A. N.; Katsnelson, M. I.; van Schilfgaarde, M.; Rösner, M.; Hofmann, P. Paramagnetic electronic structure of CrSBr: Comparison between ab initio GWtheory and angle-resolved photoemission spectroscopy. *Phys. Rev. B* **2023**, *107*, 235107.
(62) Stier, A. V.; Wilson, N. P.; Velizhanin, K. A.; Kono, J.; Xu, X.; Crooker, S. A. Magnetooptics of Exciton Rydberg States in a Monolayer Semiconductor. *Phys. Rev. Lett.* **2018**, *120*, No. 057405.
(63) Klein, J.; Hötger, A.; Florian, M.; Steinhoff, A.; Delhomme, A.; Taniguchi, T.; Watanabe, K.; Jahnke, F.; Holleitner, A. W.; Potemski, M.; Faugeras, C.; Finley, J. J.; Stier, A. V. Controlling exciton many-body states by the electric-field effect in monolayer MoS_2. *Phys. Rev. Res.* **2021**, *3*, L022009.
(64) Faria Junior, P. E.; Zollner, K.; Woźniak, T.; Kurpas, M.; Gmitra, M.; Fabian, J. First-principles insights into the spin-valley physics of strained transition metal dichalcogenides monolayers. *New J. Phys.* **2022**, *24*, No. 083004.
(65) Wang, Z.; Mak, K. F.; Shan, J. Strongly Interaction-Enhanced Valley Magnetic Response in Monolayer WSe_2. *Phys. Rev. Lett.* **2018**, *120*, No. 066402.
(66) Xuan, F.; Quek, S. Y. Valley Zeeman effect and Landau levels in two-dimensional transition metal dichalcogenides. *Physical Review Research* **2020**, *2*, No. 033256.
(67) Mitioglu, A. A.; Galkowski, K.; Surrente, A.; Klopotowski, L.; Dumcenco, D.; Kis, A.; Maude, D. K.; Plochocka, P. Magnetoexcitons in large area CVD-grown monolayer MoS2 and MoSe2 on sapphire. *Phys. Rev. B* **2016**, *93*, 165412.
(68) Arora, A.; Koperski, M.; Slobodeniuk, A.; Nogajewski, K.; Schmidt, R.; Schneider, R.; Molas, M. R; de Vasconcellos, S. M.; Bratschitsch, R.; Potemski, M. Zeeman spectroscopy of excitons and hybridization of electronic states in few-layer WSe2, MoSe2 and MoTe2. *2D Materials* **2019**, *6*, No. 015010.
(69) Koperski, M.; Molas, M. R.; Arora, A.; Nogajewski, K.; Bartos, M.; Wyzula, J.; Vaclavkova, D.; Kossacki, P.; Potemski, M. Orbital, spin and valley contributions to Zeeman splitting of excitonic resonances in MoSe2, WSe2 and WS2Monolayers. *2D Materials* **2019**, *6*, No. 015001.
(70) Goryca, M.; Li, J.; Stier, A. V.; Taniguchi, T.; Watanabe, K.; Courtade, E.; Shree, S.; Robert, C.; Urbaszek, B.; Marie, X.; Crooker, S. A. Revealing exciton masses and dielectric properties of monolayer semiconductors with high magnetic fields. *Nat. Commun.* **2019**, *10*, 1−12.
(71) Robert, C.; Han, B.; Kapuscinski, P.; Delhomme, A.; Faugeras, C.; Amand, T.; Molas, M. R.; Bartos, M.; Watanabe, K.; Taniguchi, T.; Urbaszek, B.; Potemski, M.; Marie, X. Measurement of the spin-

https://doi.org/10.1021/acs.nanolett.3c03431
Nano Lett. 2023, 23, 11073−11081

forbidden dark excitons in MoS2 and MoSe2 monolayers. *Nat. Commun.* **2020**, *11*, 1−8.
(72) Faria Junior, P. E.; Fabian, J. Signatures of Electric Field and Layer Separation Effects on the Spin-Valley Physics of $MoSe_2$ /WSe_2 Heterobilayers: From Energy Bands to Dipolar Excitons. *Nanomaterials* **2023**, *13*, 1187.
(73) Heißenbüttel, M.-C.; Deilmann, T.; Krüger, P.; Rohlfing, M. Valley-Dependent Interlayer Excitons in Magnetic WSe2/CrI3. *Nano Lett.* **2021**, *21*, 5173.
(74) Faria Junior, P. E; Naimer, T.; McCreary, K. M; Jonker, B. T; Finley, J. J; Crooker, S. A; Fabian, J.; Stier, A. V Proximity-enhanced valley Zeeman splitting at the WS2/graphene interface. *2D Materials* **2023**, *10*, No. 034002.
(75) Tedeschi, D.; De Luca, M.; Faria Junior, P. E.; Granados del Águila, A.; Gao, Q.; Tan, H. H.; Scharf, B.; Christianen, P. C. M.; Jagadish, C.; Fabian, J.; Polimeni, A. Unusual spin properties of InP wurtzite nanowires revealed by Zeeman splitting spectroscopy. *Phys. Rev. B* **2019**, *99*, 161204.
(76) Van Tuan, D.; Yang, M.; Dery, H. Coulomb interaction in monolayer transition-metal dichalcogenides. *Phys. Rev. B* **2018**, *98*, 125308.
(77) Florian, M.; Hartmann, M.; Steinhoff, A.; Klein, J.; Holleitner, A. W.; Finley, J. J.; Wehling, T. O.; Kaniber, M.; Gies, C. The Dielectric Impact of Layer Distances on Exciton and Trion Binding Energies in van der Waals Heterostructures. *Nano Lett.* **2018**, *18*, 2725−2732.
(78) Zhumagulov, Y. V.; Vagov, A.; Senkevich, N. Y.; Gulevich, D. R.; Perebeinos, V. Three-particle states and brightening of intervalley excitons in a doped MoS2 monolayer. *Phys. Rev. B* **2020**, *101*, 245433.
(79) Lin, Y.; Ling, X.; Yu, L.; Huang, S.; Hsu, A. L.; Lee, Y. H.; Kong, J.; Dresselhaus, M. S.; Palacios, T. Dielectric screening of excitons and trions in single-layer MoS2. *Nano Lett.* **2014**, *14*, 5569−5576.

https://doi.org/10.1021/acs.nanolett.3c03431
Nano Lett. 2023, 23, 11073−11081